Reflective Probing of the Electrical Conductivity of Hot Aluminum in the Solid, Liquid, and Plasma Phases

Andrew N. Mostovych[1] and Yung Chan[2]
[1]*Laser Plasma Branch Plasma Physics Division, U.S. Naval Research Laboratory, Washington, D. C. 20375*
[2]*Science Applications International Corporation, McLean, Virginia 22102*
(Received 23 August 1996)

The physics of dense aluminum in transition between metallic and insulating states of the solid, liquid, and plasma phases is probed in thermally equilibrated, inertially confined, laser heated targets. Time resolved laser probes measure the reflectivity of thin aluminum layers embedded inside the target. The electrical conductivity is inferred from the reflectivity with a free-electron Drude conduction model. It is found to be sharply below liquid aluminum values and differs by at least an order of magnitude from current theoretical predictions. [S0031-9007(97)04692-9]

PACS numbers: 72.15.Cz, 52.25.Fi, 71.30.+h, 78.20.Ci

For most nonalkali metals, measurements of the electrical and thermal properties are limited to the low temperature ($<$2000 K) near-solid density ($N \sim N_{\text{solid}}$) condensed state or to the high temperature ($>$10000 K), low-density ($N \ll N_{\text{solid}}$) gas and plasma states. Calculations in the ordered solid and liquid phases and the highly disordered gas phase lend themselves to simplifying assumptions, whereas calculations in the transition between these phases are difficult. In this transitional regime, dense hot matter is typically degenerate and strongly coupled. Experimental data are limited. Most are due to high-intensity reflectivity experiments with short-pulse laser heating of solid targets. The laser pulse lengths were typically shorter than 0.5 psec in order to prevent hydrodynamic expansion of the targets [1]. Unfortunately, the equilibration time between the solid lattice and the laser-heated electrons was typically longer or of the same order as the laser pulse length, thus thermal equilibrium could not be assured and the thermal state of the solid lattice was not well known.

In this Letter, we report on experiments with tamped laser-heated aluminum which succeeded in preparing aluminum in the transitional regime ($N \sim 0.5-1.0 N_{\text{solid}}$; $T \sim 0.3-1.0$ eV) 3500–11000 K) under conditions of thermal equilibrium and at sufficiently high pressure to be well above the predicted critical point pressure and boiling curve for aluminum. In contrast to the earlier short-pulse experiments [1], thermal equilibrium is assured by the long lifetime of the experiment ($\tau \geq 1000$ psec) in relation to typical lattice equilibration times ($\tau_{\text{eq}} \sim 1$ psec) and the state of the aluminum is determined by independent measurements of temperature and pressure. The electrical conductivity is measured by reflective probing. We find that the conductivity falls sharply as the aluminum is heated above 0.4 eV, substantially deviating from extrapolations of liquid-metal theory and from the known behavior of liquid aluminum near the melting point. The conductivity falls to levels consistent with a state of "minimum metallic conductivity" and the metal-insulator transition [2]. This reduction is observed at temperatures at least an order of magnitude lower than where the short-pulse experiments exhibit significant changes in reflectivity. Recent theoretical predictions [3–5], based on generalized Ziman models and strongly coupled plasma theory, do not match the data, differing by at least an order of magnitude. Previous work with electrical discharges in metallic wires [6] had shown reasonable agreement with liquid-metal theory below 0.4 eV but resistivity measurements above this point were not possible because the discharges became unstable and fully disrupted. Our work may explain these disruptions, given the sharp fall in conductivity we observe at temperatures coincident with the disruption point.

Solid aluminum at temperatures near or above 5000 K generates very high pressures ($\sim$100 kbar) which, if unconfined, will very quickly decompress to low gas-phase densities. We use laser heating of special tamped targets [7] to dynamically confine aluminum samples imbedded in the target interior. Figure 1 shows a typical target. A thin layer of aluminum (0.1, 0.25, 0.5, and 1.0 μm) is deposited on a fused silica substrate and tamped with a second fused silica substrate. High quality tamping is insured by using a fluid gasket (distilled water) to completely fill the space in a thin, well-defined gap (200 μm) between the aluminum layer and the second substrate. A moderate intensity laser beam ($\lambda = 1.054$ μm, $d \approx 1$ mm, $I \sim 10^9 - 10^{10}$ W/cm^2) is focused through the uncoated substrate, through the water, and on to the aluminum layer. The laser is strongly absorbed in about the first skin depth in the aluminum, heating it to temperatures in the 1–4 eV range. Adjoining water layers also ionize and become strongly heated by the laser. The hot aluminum and water generate a shock wave which pressurizes the aluminum layer but does not substantially heat it at the SiO_2-Al interface. The interface region sees substantial heating (0.3–1.0 eV) only as a result of thermal conductions from the front surface.

The heated aluminum is diagnosed with temporally and spatially resolved diagnostics which measure the front (laser heating side) and rear temperatures, the target pressure, and the reflectivity of the Al-SiO_2 interface.

 0031-9007/97/79(25)/5094(4)$10.00

Temperature is determined from absolute emission measurements from the Al-SiO_2 interface and a measurement of the surface emissivity ($\varepsilon = 1 - R$ where R is the target reflectivity at the emission wavelength). Typically, the measured rear side temperatures are in the 0.3–1.0 eV range while the front surface, directly heated by the laser, is in the range of 1.0–3.0 eV. The 0.3 eV limit corresponds to limits in the detection sensitivity, while the high temperature limits are due to limits on the energy that can be deposited in the aluminum layer. Pressure in the target is deduced from the relationship between the particle velocity and the pressure behind a weak shock front [8]. As shown in Fig. 1, a time-resolved laser interferometer is used to measure the position and velocity of the Al-SiO_2 interface as the SiO_2 is compressed in response to the pressure in the target. In all cases the measured phase shift is corrected for changes in the index of refraction (roughly 10%) of SiO_2 as the result of compression. For the conditions of this experiment the pressure is in the range of 30–100 kbar, well above the predicted critical pressure (~7 kbar) for aluminum [9].

The reflectivity is measured with a set of 0.527 μm laser probes which are focused and reflected from a target at 6° and 45° with S and P polarizations. The rear surface of the target is wedged to prevent interference from multiple reflections from the rear surface of the SiO_2 substrate. The laser probes are pulsed and contain two temporally stacked pulses such that a reference pulse reflects from the target just before the target is heated. A probing pulse is then synchronized to reflect during the time of heating. A set of fast photodiodes detects the reflected probes. Figure 2 shows typical temperature and reflectivity data for targets with thick and thin aluminum layers. The reflectivity falls sharply as the interface temperature approaches 0.4 eV. For the thin-layer targets (0.1 μm), where the thermal conduction times (~0.25 ns) and the shock transit times (~0.025 ns) are shorter than the laser duration, the temperature rise and the fall in reflectivity occur at the moment of laser heating. For thick-layer targets (1.0 μm) the thermal conduction times (~10 ns) are much longer than the shock transit time (0.25 ns) and no change in reflectivity is detected during the time the interface is at high pressure but before heating by thermal conduction. We find that changes in reflectivity correlate with increases in the temperature of the aluminum layer but not with increases of the internal target pressure.

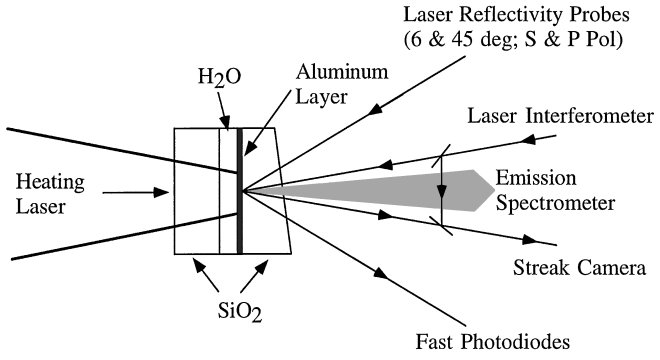

FIG. 1. Schematic of tamped targets and diagnostics. Pulsed laser probes at 6° and 45° measure aluminum layer reflectivity while an absolutely calibrated spectrometer is used to measure the target temperature. Target pressure is inferred from the Al-SiO_2 interface velocity, measured by laser interferometry.

Measurements of reflectivity as a function target temperature are displayed in Fig. 3. Upon heating, the reflectivity drops to about 20% of the original reflectivity. Most of the drop occurs in a narrow temperature range between 0.3 to 0.5 eV, with little additional change at higher temperatures. Within experimental error, no discernible difference is observed in the reflectivity at 6° and 45° between either the S or P polarization. For comparison to theory it is convenient to infer an electrical conductivity from the reflectivity. The Drude conduction model for the high-frequency conductivity $\sigma = \sigma_0(1 - i\omega\tau)^{-1}$ ($\sigma_0 = \mathrm{Ne}^2\tau/\mathrm{m}$ is the dc conductivity, τ is the collisional relaxation time, and N is the free electron density) is used to relate the dc conductivity to the high-frequency conductivity, the complex index of refraction, and ultimately the reflectivity [10]. The curves in Fig. 3 show sample calculations of the reflectivity from an Al-SiO_2 Fresnel interface, at constant aluminum density, as a function of the relaxation time $\tau/\tau_{\mathrm{Al(STP)}}$, where $\tau_{\mathrm{Al(STP)}}$ is the relaxation time under standard conditions. Aluminum is assumed to be a simple-free-electron Drude-metal with no interband contributions to the conductivity. Previous experiments with liquid aluminum have verified this assumption for visible wavelengths [11]. The Drude model cannot extend to arbitrary short relaxation times. For conduction electrons, degenerate, and moving with the Fermi energy, the "uncertainty principle" ($\Delta X \Delta P \geq \hbar/2$)

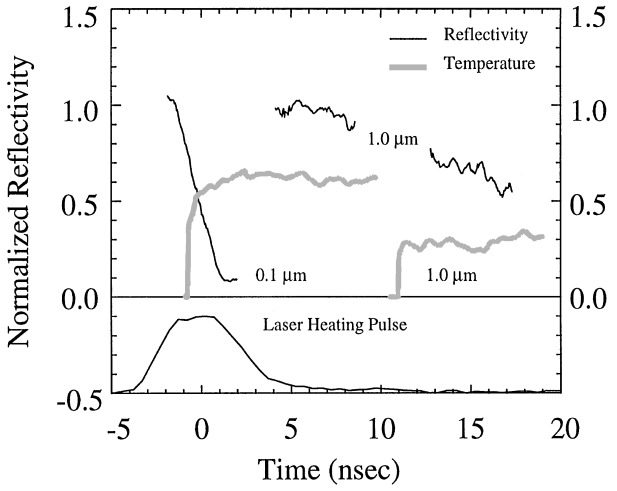

FIG. 2. The time history of the aluminum rear-side temperature and reflectivity for 0.1 and 1.0 μm thick aluminum layers. The rise in temperature and fall in reflectivity occurs at the time of heating for thin layers while for 1.0 μm thick layers these changes are delayed by thermal conduction for about 10 nsec. Changes in reflectivity correlate with increased temperature but not with increases in target pressure

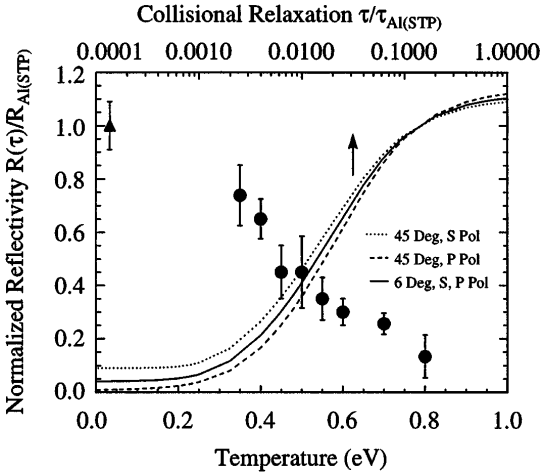

FIG. 3. Measured reflectivity (S Pol @ 6°) as a function of target temperature. Each data point corresponds to an average over several shots (3–5) and the error bars are due to the standard deviation of the mean. Measurements at room temperature (diamond data point) agree with calculated reflectivity values for aluminum. Curves due to calculations of the Al-SiO_2 interface reflectivity as a function of relaxation time for aluminum with three free electrons. The Drude free-electron model is used to model the conductivity.

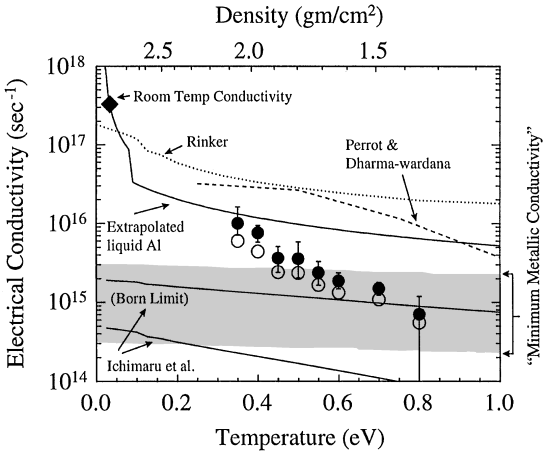

FIG. 4. Electrical conductivity of heated aluminum as a function of temperature and density. It is inverted from the reflectivity of the heated aluminum as per Fig. 3. Above 0.3 eV the conductivity falls sharply and enters a region associated with the metal-insulator transition and "minimum metallic conductivity." Solid data points are inverted with $Z = 3$ while the open circles correspond to $Z = 1$.

limits the interaction time of elastic collisions to $\Delta\tau \geq \hbar/(8E_F) \approx 0.001\tau_{\mathrm{A1(STP)}}$. As a result, the very lowest reflectivity data may not be well modeled by the Drude model.

In practice, the target density is not constant and a separate reflectivity curve is calculated for each density in the experiment. The reflectivity curves are inverted, resulting in Fig. 4 where the dc conductivity is displayed (solid points) as a function of target temperature and density. For simplicity, only the more accurate 6° reflectivity data are used in this analysis. The Sesame equation-of-state tables [12] are used to determine the aluminum ion density from the measured temperature and pressure ($P = 60 \pm 20$ kbar for data in Fig. 4). The number of free electrons is set to three-per-ion as per the valence of aluminum metal. This is done because $Z = 3$ is the expected valence of aluminum at densities above those of the metal-insulator transition. This choice permits easy comparison of the data to the different theoretical models, most of which differ in calculations of the average ionization. The reflectivity-to-conductivity conversions are not particularly sensitive to this choice as evidenced by the second data set (open circles) which is inverted with only one free electron per ion. The error bars include the uncertainty of the reflectivity measurement as well as the uncertainty of the target density. Typically, the uncertainty in the temperature measurement is less than ± 0.05 eV.

The Fresnel interface assumption is very demanding. As was found in earlier short-pulse experiments with free-surface solid targets, finite gradients in the index of refraction quickly produce deviations from the reflectivity given by the sharp Fresnel interface solutions [1]. The applicability of the Fresnel assumption for this experiment, where the reflecting surface is tamped, was checked by solving the wave equation for the class of index-of-refraction gradients that could be expected in our targets. In the aluminum layer the state of the material and the refraction index varies primarily as a result of the temperature gradient. For a constant thermal diffusivity (average value measured in experiment) and an electrical conductivity dependence as in liquid aluminum [13] the change in reflectivity is less than a few percent as a result of these gradients. The true gradients in temperature and refractive index of the aluminum at the interface should be flatter than is calculated because the thermal diffusivity is, in fact, strongly dependent on temperature, falling orders of magnitude as solid aluminum transitions to the liquid and plasma states in the laser heated regions. On the SiO_2 side, the refractive index is almost completely real. As an insulator, SiO_2 has negligible free electrons but a small number of electrons can be produced by thermal ionization (calculations give ionizations of less than 0.1% at 0.5 eV). This ionization produces a gradient in the SiO_2 refractive index which is of the same order as the thermal diffusion scale length into the SiO_2. Using layered targets, the average thermal diffusivity of SiO_2 was also measured in these experiments. We find that the thermal diffusivity is sufficiently low (~ 0.025 cm^2/sec) such that the SiO_2 refractive index gradient has a scale length of less than 0.1 μm and the reflectivity from the Al-SiO_2 interface is not modified by more than a few percent. It is unlikely that the sharp drop in reflectivity results from gradients at the interface but instead is due to the conductivity properties of aluminum at these elevated temperatures.

At low temperatures (~ 0.35 eV), the measured conductivity is in agreement with "standard liquid metal"

Ziman type calculations [14] and lies on the curve (solid line, Fig. 4) extrapolated from tabulated conductivities of liquid aluminum from near the melting point [13]. At higher temperatures the conductivity falls sharply and enters a region associated with a "minimum metallic conductivity" and the metal-insulator transition [2]. This is represented in Fig. 4 by the thick shaded region bounded from the top by the Ioffe-Regel condition [mean free path = interion spacing; $\sigma_{\mathrm{IR}} = e^2/3\hbar a$ where $a = (3/4\pi N)^{1/3}$] and from the bottom by an Anderson-Localization "minimum conductivity" ($\sigma_{\min} \approx 0.03e^2/\hbar a$). It is likely that the point of localization will also represent the limit of characterizing the aluminum as a free-electron metal.

Calculations of conductivity for dense systems are typically based on variations of the Ziman formula [15]

$$\sigma^{-1} \propto \int_0^\infty dk\, k^3 f_o\left(\frac{k}{2}\right) \left| \frac{V_{ei}(k)}{\varepsilon(k)} \right|^2 S_{ii}(k)\,.$$

V_{ei} is electron-ion interaction potential, ε is the dielectric function, f_0 the Fermi distribution function, and S_{ii} is the ion structure factor. For liquid metals near the melting point the Ziman formula is usually solved with a parametric pseudopotential and a hard or soft sphere model for the ion structure factor [14]. This simplified approach is not self-consistent, but along with neutron scattering measurements of the structure factor and experimental determinations of the potential parameters it was adequate to prove the general validity of the Ziman formula. A more general theoretical approach is needed for more highly disordered systems at elevated temperatures. We compare several recent generalized calculations to our data. The top dotted curve is due to Rinker [3]. This calculation is an "average-atom", partial-wave formulation of the Ziman theory. The electron states and interaction cross sections are calculated self-consistently but the ion structure factor is taken from independent calculations for one-component plasmas. The dashed curve is due to the density-functional, neutral pseudoatom model of Perrot and Dharma-wardana [4]. The ion-electron interactions and the structure factor are calculated self-consistently within the framework of density-functional theory and the average-atom model. Both calculations predict conductivities which are at least an order of magnitude larger than those measured. In contrast, the calculations in the bottom curve are about an order of magnitude too low. These calculations are due to Ichimaru *et al.* [5] for hydrogen plasmas. The Z dependence is incorporated via separate calculations of ion-sphere-model cross sections. For the comparisons in this work $Z = 3$, as per the valence of aluminum. These calculations predict low conductivities as a result of the formation of "incipient Rydberg states" (IRS) in regions of very strong ion-electron coupling. Formally, these are extrapolations onto the parameter space of the experiment because the validity range of the calculations is limited to lower coupling strengths ($0.05 < \Gamma < 43.4$) than are found in this experiment ($60 < \Gamma < 250$). If the theory is applied in its Born limit ($E_F > mZ^2e^4/2\hbar^2$), then the IRS states are turned off and the agreement with experiment is good at the higher temperatures. Apparently, the IRS states do not transition to metallic conduction-band states at the higher coupling strengths.

The reflectivity of aluminum in the vicinity of the metal-insulator transition has been measured with tamped laser-heated targets. The electrical conductivity inferred through a Drude free-electron model show major (order of magnitude) disagreements between theory and experiment. In addition, this work suggests anomalous behavior for any electrical discharges where the current carrying conductors are heated much beyond the melting point.

This work was supported by the U.S. Office of Naval Research.

[1] Some resent reflectivity experiments with short pulse lasers: D. F. Price *et al.*, Phys. Rev. Lett. **75**, 252 (1995); X. Y. Wang and M. C. Downer, Opt. Lett. **17**, 1450 (1992); R. Fedosejevs *et al.*, Appl. Phys. B **50**, 79 (1990); H. M. Milchberg *et al.*, Phys. Rev. Lett. **61**, 2364 (1988).

[2] N. F. Mott, *Metal-Insulator Transitions* (Taylor & Francis, New York, 1990).

[3] G. A. Rinker, Phys. Rev. A **37**, 1284 (1988); G. A. Rinker, Phys. Rev. B **31**, 4207 (1985).

[4] F. Perrot and M. W. C. Dharma-wardana, Phys. Rev. E **52**, 5352 (1995).

[5] H. Kitamura and S. Ichimaru, Phys. Rev. E **51**, 6004 (1995); S. Tanaka, X. Yan, and S. Ichimaru, Phys. Rev. A **41**, 5616 (1990).

[6] G. R. Gathers, Rep. Prog. Phys. **49**, 341 (1986); G. R. Gathers and M. Ross, J. Non-Cryst. Solids **61 & 62**, 59 (1984); S. V. Lebedev, High Temp. (USSR) **19**, 219 (1981).

[7] Similar to targets used in early laser confined-shock experiments; L C. Yang, J. Appl. Phys. **45**, 2601 (1974); B. P. Fairand and A. H. Clauer, J. Appl. Phys. **50**, 1497 (1979); P. E. Schoen and A. J. Campillo, Appl. Phys. Lett. **45**, 1049 (1984).

[8] Ya. B. Zeldovich and Yu. P. Raizer, *Physics of Shock Waves and High-Temperature Hydrodynamic Phenomena* (Academic Press, New York, 1964).

[9] G. I. Kerley, Sandia Report No. SAND88-2291-UC-405, 1991 (unpublished); A. V. Bushman and V. E. Fortov, Sov. Technol. Rev. B, Therm. Phys. **1**, 219 (1987).

[10] M. Born and E. Wolf, *Principles of Optics* (Pargamon Press, New York, 1980).

[11] J. C. Miller, Philos. Mag. **20**, 1115 (1969).

[12] S. P. Lyon and J. D. Johnson, Los Alamos Report No. LA-UR-92-347, 1991 (unpublished).

[13] Extrapolated from tabulated values, in G. T. Dyos and T. Farrell, *Electrical Resistively Handbook* (Peter Peregrinus Ltd., London, 1992).

[14] N. W. Ashcroft and J. Lekner, Phys. Rev. **145**, 83 (1966).

[15] J. M. Ziman, Philos. Mag. **6**, 1013 (1961).